



pH-Dependent Aggregation and pH-Independent Cell Membrane Adhesion of Monolayer-Protected Mixed Charged Gold Nanoparticles

Journal:	<i>Nanoscale</i>
Manuscript ID	NR-ART-11-2018-009617.R3
Article Type:	Paper
Date Submitted by the Author:	18-Mar-2019
Complete List of Authors:	Shen, Zhiqiang; University of Connecticut, Mechanical Engineering Baker, William; University of Arkansas, Department of Biomedical Engineering Ye, Huilin; University of Connecticut, Li, Ying; University of Connecticut System, Mechanical Engineering

Cite this: DOI: 10.1039/xxxxxxxxxx

pH-Dependent Aggregation and pH-Independent Cell Membrane Adhesion of Monolayer-Protected Mixed Charged Gold Nanoparticles[†]

Zhiqiang Shen^{‡, a}, William Baker^{‡, b}, Huilin Ye,^a and Ying Li,^{*a}

Received Date

Accepted Date

DOI: 10.1039/xxxxxxxxxx

www.rsc.org/journalname

Design of pH-responsive monolayer-protected gold nanoparticles (AuNPs) that are mixed charged with the ability to switch its net surface charge based on the stimuli of environmental pH is a promising technique in nanomedicine. However, understandings of the pH-responsive mixed charged AuNPs behaviors in terms of their stability and cellular interaction are still limited. In this work, we study the aggregation of pH-responsive AuNPs and their interaction with model lipid bilayers by adopting the Martini coarse-grained (CG) molecular dynamics simulations. The surface of these AuNPs is decorated by the both positively and negatively charged ligands. The AuNP is positively charged at low pH values due to protonation of negatively charged ligands. Its net charge is lowered at higher pH by increasing the ratio of deprotonated negative charge ligands. We find that the AuNPs are severely aggregated at moderate pH value, where each AuNP has overall neutral charge, and they are stable and dispersed at both low and high pH values. Further free energy analysis reveals that the energy barrier before the location of hydrophobic driving force potential well plays the key role that determines the stability of monolayer-protected AuNPs at different pH values. This energy barrier is dramatically decreased at moderate pH value, leading to the severe aggregation of AuNPs. By investigating the interaction between AuNPs and model lipid bilayers, we find that all the AuNPs adhere onto the lipid bilayer, independent of the pH value. Moreover, the lipids originally in the bilayer are extracted by these AuNPs through a process of protrusion and upward climbing. The extraction of lipids can cause dehydration and disruption of bilayers, when multiple AuNPs adhered. Free energy analysis reveals that the penetration of AuNPs will induce dramatic free energy increment because of deformation of ligands with hydrophilic functional end groups. We have systematically studied the stability of pH-responsive AuNPs and their interactions with lipid bilayers in simulation, which might pave the way for the design of pH-responsive monolayer protected AuNPs for biomedical applications.

1 Introduction

Monolayer-protected gold nanoparticles (AuNPs) have wide applications in nanomedicine as drug delivery vehicles^{1,2} and nanothermal^{3–5} and diagnostic^{6,7} agents. Particularly, AuNPs featured with the unique electronic, optical and biocompatible properties stand themselves out among various NP candidates^{8,9}. Furthermore, the gold NP surface can be easily passivated by Au-S co-

valent bonds that facilitate the decoration of sulfur-containing organic molecules on AuNPs core to form the monolayer-protected surface with tunable hydrophobicity and electronic charge¹⁰. In the setting of nanomedicine, it is desirable for the NPs to circulate along with the blood flow through the vascular network, passively accumulate in tumor sites through the enhanced permeation and retention (EPR) effect, and adhere onto or uptaken by tumor cells¹¹. One of the key challenges in nanomedicine is the low delivery efficiency of NPs to solid tumors¹². For instance, only 0.7% of injected NPs on average are successfully delivered to tumor sites in mouse models¹³. Therefore, the design of NP surface properties, which determine NPs' interactions with biological environments, is crucial to improve the efficacy of nanomedicine^{14–18}.

Design of NPs that are responsive to the pH of the local biological environment in the human body is a promising strategy to

^a Department of Mechanical Engineering and Institute of Materials Science, University of Connecticut, Storrs, CT 06269, USA. Fax: +1 860 4865088; Tel: +1 860 4867110; E-mail: yingli@engr.uconn.edu

^b Department of Biomedical Engineering, University of Arkansas, Fayetteville, AR 72701, USA.

[†] Supporting Information (SI) available: Details of the computational models for lipid membrane and monolayer protected AuNPs, and additional simulation results. See DOI: 10.1039/b000000x/

[‡] These authors contributed equally.

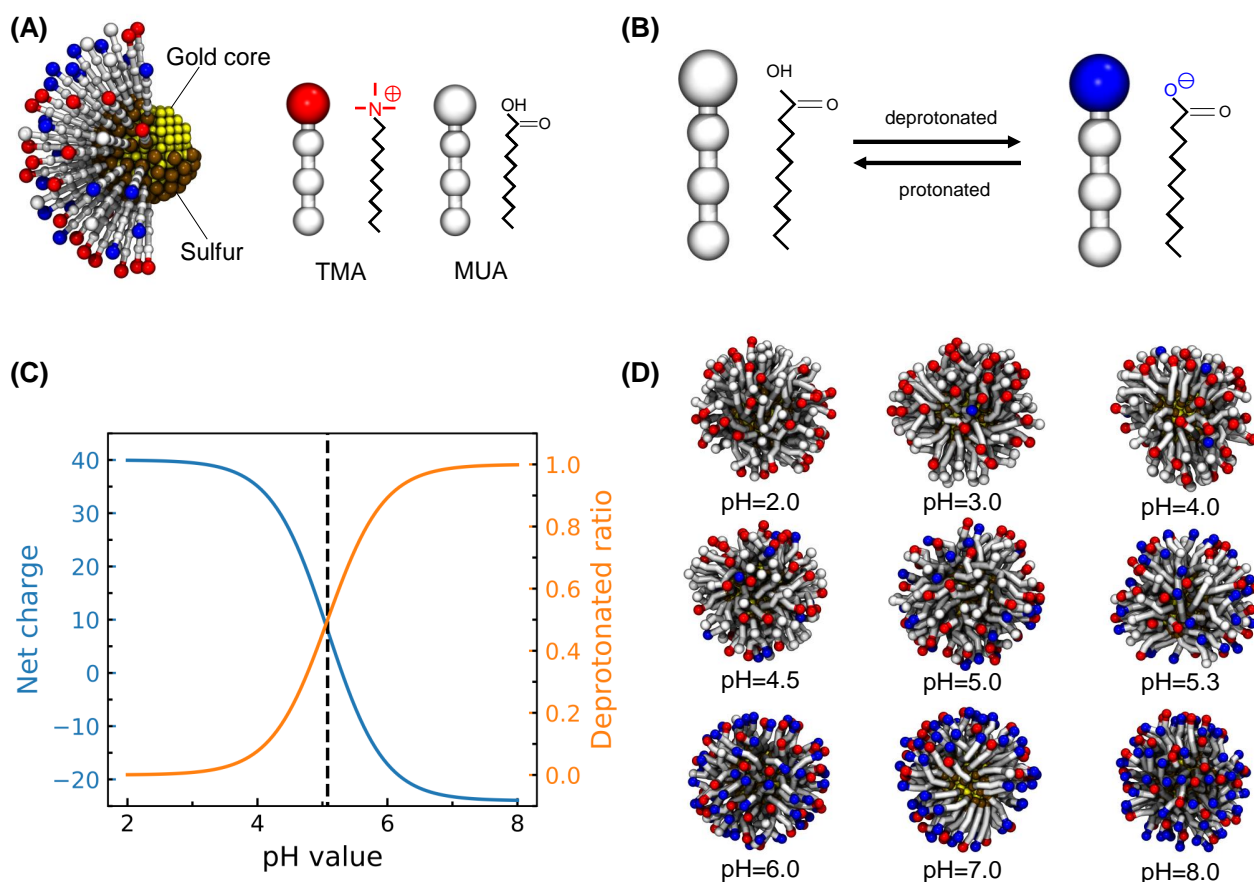


Fig. 1 Computational model. (A) Components of the monolayer protected AuNPs. The yellow beads represent the Au core. The tan beads represent the sulfur atoms that cover the Au core. Two different ligands are tethered on Au surfaces; the N,N,N-trimethyl(11-mercaptoundecyl)ammonium ion (TMA) is composed of an alkane chain (colored in white) and a terminal functionalized with a positive, protonated amino group ($-\text{NH}_3^+$) (colored in red). The other is the 11-mercaptoundecanoic acid (MUA) ligand, which consists of an alkane chain and its neutral carboxyl terminal ($-\text{COOH}$). (B) The carboxyl group in MUA can be deprotonated at high pH and becomes negative (colored in blue). (C) The curves of deprotonated ratio of MUA and the AuNP's net charge against the pH value. The dash line in the figure denotes the location of pKa value of MUA. (D) Relaxed configuration of AuNPs at a series of different pH values.

enhance NP delivery efficiency^{15,19–21}. The human body shows quite a range of pH values in the micro-environment at the tissue level. For instance, the pH of normal healthy tissue is $\text{pH} \approx 7.4$ ²². The micro-environment around a tumor, however, has a much lower pH, around 6.5 ²³. A pH-responsive NP could smartly respond to the proton concentration at different pH values so that it can achieve an extension of circulation time and enhanced internalization by tumor cells²⁰. In the designs of pH-responsive NPs, utilizing the mixed charged monolayer-protected AuNP to switch its net surface charge based on the stimuli of environmental pH is one of those promising techniques^{15,20,24}. For instance, Pillai et.al.²⁵ designed a AuNP tethered with two different ligands: N,N,N-trimethyl (11-mercaptoundecyl) ammonium ion (TMA) and 11-mercaptoundecanoic acid (MUA). The TMA is always positively charged, while the pKa of MUA is 5.08. Therefore, the MUA can be neutral or negatively charged depending on its protonation or deprotonation at low or high pH values. The monolayer-protected AuNPs in their experiments are negatively charged at high pH value and positively charged at low pH, which facilitate their stability and promote cellular uptake efficiency.

Although the strategy of engineering pH-responsive monolayer protected AuNPs is promising, understandings of the behaviors of pH-responsive mixed charged AuNPs in terms of their stability and cellular interaction are still limited.^{25–28}

Good stability or dispersity of NPs in a biological environment is one of the primary properties of NPs for extended blood circulation^{29,30}. Moreover, the aggregation of NPs may induce toxicity and reduce the NP delivery efficiency³¹. In experiments, Grzybowski et.al.^{32,33} found that oppositely charged monolayer protected AuNPs with different sizes and charge ratios express 'ionic-like' stability: these opposite charge AuNPs are stable in solution and precipitate only at a threshold point that is determined by the condition of electroneutrality. On the other hand, it is found that the same signed-charge AuNPs might aggregate and precipitate in solution despite their electrostatic repulsion^{34,35}. In theory, as pointed in Ref³⁶, the Derjaguin-Landau-Verwey-Overbeek (DLVO) theory, which is used to predict the aggregation behavior of charged colloidal particles^{37,38}, might not be useful, due to the contradiction between its continuum assumption and the small size of AuNPs ($< 10 \text{ nm}$). Therefore, computational simula-

tions are applied to explore the molecular details and the physical mechanism for aggregation. For instance, Lin et.al.³⁹ found that the aggregated cluster morphology of monolayer-protected AuNPs is largely determined by the tethered hydrophobic ligand length by using the Martini coarse-grained (CG) model. Lehn et.al.³⁶ adopted an implicit solvent model to study the free energy change of two identical anionic monolayer protected AuNPs. They found that the aggregation of these AuNPs is driven by the short-range hydrophobic attraction. However, the effect of charged groups on aggregation behaviors of AuNPs is not clear. Furthermore, to the best of our knowledge, no simulation has been done to make a one-to-one comparison between the aggregation behavior of AuNPs and the corresponding free energy change between two AuNPs. Therefore, it is difficult to correlate the phenomena in cluster formation of AuNPs to the physical mechanisms about energy barrier and driving force.

Cellular uptake efficiency of AuNPs is another aspect to determine the overall efficacy of NPs. Due to the fact that tumor cell membranes are negatively charged, some experimental evidence shows that cationic NPs are more efficient to be uptaken compared to their anionic counterparts^{25,40–42}. However, it has also been proven in experiments that cationic AuNPs might be cytotoxic and disruptive by inducing hole formations in membranes and membrane thinning^{43–45}. In simulation, Lehn et.al.^{46,47} found that free energy change for AuNP penetration into bilayer is a result of competition between the hydrophobic driving force provided by the favorable interaction between alkane chain and lipid tail and the energy penalty induced by the end functional group snorkeling. They also proposed that the kinetic pathway of AuNPs insertion is initiated by the protrusion of lipids, which form the first contact between the alkane chain and lipid tails that facilitates the insertion of AuNPs⁴⁸. Lin et.al.⁴⁹ also investigated the interaction between lipid bilayers and AuNPs with different signs and densities of surface charge. They found that the AuNPs show either repulsive, adhesive, or penetrating behavior toward the lipid bilayers, when their surface changed from negatively to positively charged. Especially, a defective area was founded in bilayer when the AuNP was highly positive. Though numerous simulation works have been done, the molecular details of the interaction between monolayer protected AuNPs and lipid bilayers is not fully understood. For instance, it is still unclear how non-inserted AuNPs can cause the dehydration of lipid bilayer, which is associated with the decreasing of the area per lipid and the bilayer thickness⁴⁴. Furthermore, few works have been published to clarify the interaction between lipid bilayers and pH-responsive mixed charged AuNPs.

In views of the importance of pH-responsive monolayer protected AuNPs in drug delivery, we utilize the Martini CG model to understand their stability in solution and interaction with tumor cells. Particularly, the monolayer protected AuNP contains two different ligands (cf.Fig.1.A). The first is positively charged TMA, and the other is MUA with $pK_a = 5.08$. Therefore, in a low pH environment, the MUA is neutral. While, at a high pH, its carboxyl end group is deprotonated, resulting in a negatively charged MUA. With a ratio of TMA:MUA=1:1.6, the AuNPs are positively charged at low pH and negatively charged at high pH.

We firstly investigate the aggregation behavior of AuNPs at different pH values. Then, a series of one-to-one comparisons about free energy analysis associated with the aggregation at different pH are performed. It is interesting to find that the AuNPs show server aggregated state at moderate pH near the pK_a value of MUA and are dispersed at low or high pH. Furthermore, two different correlated states between AuNPs are found within the aggregated cluster. These two different states are caused by two different minimum values existing in the potential of mean force (PMF) between AuNPs. Interestingly, instead of the global minimum caused by the hydrophobic attraction between ligands, the energy barrier before it determines the aggregation of AuNPs. Additionally, we further explore the interaction between AuNPs and the negatively charged model lipid bilayers at different pH values. Both unbiased and free energy analysis simulation are performed. With all the terminals are functionalized, we find that no AuNP can penetrate into the bilayer, which will cause a dramatic free energy increment due to the hydrophilic ends. Instead of penetrating, all of the AuNPs adhere on the lipid bilayer. Moreover, the AuNPs can extract up to 10 lipids from the lipid bilayer. This extraction of lipids follows a protrusion and climbing up process, which might be able to explain the lipid bilayer dehydration if multiple AuNPs exist. Our simulations systematically study the stability of pH-responsive AuNPs and their interaction with model lipid bilayers, which might pave the way for the design of pH-responsive monolayer protected AuNPs for biomedical applications.

2 Computational Model and Methods

The Martini CG force field^{50,51} is adopted in our work to investigate the aggregation and bilayer interaction process of pH-responsive monolayer-protected AuNPs. In the Martini force field, 3 or 4 heavy atoms are treated as one CG interactive bead. The Martini force field is particularly suitable for studying the biomolecular systems, which has been parameterized in a systematic way, combining top-down and bottom-up strategies. The non-bonded interactions are derived from the top-down approach by reproducing the experimental partition free energies between polar and apolar phases of a large number of chemical species; while all the bonded interactions are obtained by the bottom-up approach, derived from reference all-atom molecular simulations. Therefore, the conformation, dynamics, mechanical properties and free energy profile of different lipids and molecular species can be correctly reproduced by the Martini force field in the CG molecular dynamics simulations^{50,51}. The Martini force field has been extensively used to study biomolecules such as lipids⁵², proteins⁵³, and polymers⁵⁴. It has recently been widely applied for investigating problems related to NP-NP^{39,55} and NP-membrane^{49,56} interactions.

The model of AuNP used in our simulations is adopted from Ref⁴⁹, which could reproduce the structure and dynamic properties of Au core in experiment. The Au core of the NP is cut out of a bulk FCC lattice with a constant of 0.408 nm⁵⁶. The gold core is a truncated-octahedron with a diameter around 2.2 nm. Two different ligands are tethered on each NP by binding with the sulfur beads on the surface of Au core. One is the TMA that is composed

of an alkane chain with its positive protonated amino terminal group ($-\text{NH}_3^+$). The other ligand is MUA consisting of an alkane chain and a terminal carboxyl group ($-\text{COOH}$) (cf. Fig.1.A). There are 104 ligands in total on the AuNP surface, with the ratio of TMA:MUA = 1 : 1.6. The TMA ligand is always positive in all simulation cases, while MUA can be neutral or negatively charged, due to its $\text{pK}_a = 5.08$ ²⁵. Correspondingly, the deprotonated ratio of MUA can be calculated as⁵⁷:

$$x = 1 - \frac{10^{\text{pK}_a - \text{pH}}}{1 + 10^{\text{pK}_a - \text{pH}}} \quad (1)$$

where x is the deprotonated ratio, which corresponds to the number of deprotonated MUA ligands on the AuNPs surface in simulation. Under these parameters, the deprotonated ratio and the net charge of AuNPs are presented in Fig.1.C. At the low pH, no MUA is deprotonated and the AuNPs surface is positively charged. With the increment of pH value, the number of deprotonated negatively charged MUA increases. The AuNPs surface at high pH is mixed with positive and negative functional groups and possesses overall negative charge after the $\text{pH} = 5.3$. To systematically explore the effect of pH-responsive ligands on the monolayer protected AuNP, 9 different pH values are investigated: $\text{pH} = 2.0, 3.0, 4.0, 4.5, 5.0, 5.3, 6.0, 7.0, 8.0$. As we can see in Fig.1.D, at $\text{pH} = 2.0$, the AuNP has a highly positive charge of +40. At $\text{pH} = 5.3$, 62% of MUA ligands are deprotonated and the AuNP has overall zero net charge. At the high pH of 8.0, all of the MUA ligands are deprotonated and the AuNP has a negative charge of -24. The diameter of the monolayer-protected AuNPs is around 5.5 nm at the relaxed state. The interactive parameters under the framework of Martini force-field for the monolayer-protected AuNPs are given in Table S1 of the Support Information. Particularly, the hydrophobic Au core beads are represented by C5 type bead. The sulfur beads are neutral and represented by N0 type. The alkane chain of MUA/TMA ligands is represented by three C1 type beads. The functional group of MUA/TMA is Qda type for their hydrophilic properties⁵⁸. Moreover, the functional group on TMA possesses +1 charge. The functional group on MUA has -1 charge when deprotonated and no charge when protonated. The interactive beads within each ligand are connected using the bond potential, and the Au core with sulfur surface is treated as a rigid body in the simulations. All of these parameters are taken from the previous study⁴⁹. To mimic the negatively charged tumor membrane, the lipid bilayer used in our simulations consists of negatively charged 1,2-dipalmitoyl-sn-glycero-3-phospho-(1'-rac-glycerol) (DPPG) and neutral 1,2-dihexadecanoyl-sn-glycero-3-phosphocholine (DPPC) phospholipids. The lipid bilayer in our simulations has total lipid count of 800, with the ratio of DPPG:DPPC = 5 : 1. Please refer to reference⁵¹ for the details of the interactive parameters of lipid and water bead.

To construct the free energy profiles that determine the aggregation and penetration of AuNPs, the umbrella sampling method is used⁵⁹. Specifically, when calculating the free energy change between two AuNPs, a harmonic potential $U = \frac{1}{2}k(\zeta - \zeta_0)^2$ is applied on the center-of-mass (COM) of two AuNPs to push them towards each other. The force constant is $k = 5 \text{ kcal/mol}$. ζ denotes the distance between COMs of these two NPs. A series of win-

dows were performed at different values of ζ_0 . The width of each window is taken as 0.1 nm to ensure the overlap of NPs positions at two constitutive windows⁴⁹. The weighted histogram analysis method (WHAM) is adopted to calculate the corresponding free energy change⁶⁰. A similar procedure is utilized to estimate the free energy change during penetration of AuNPs through lipid membrane. During the penetration, ζ represents the distance between the COM distances of NP and the lipid bilayer in the direction perpendicular to the bilayer plane. In both cases, each window lasts for 30 ns in order to allow relaxation and acquire enough configurations. As we can see in Fig.S2 in Support Information, the potential of mean force (PMF) is already converged at 24 ns. The temperature in all of the simulations is controlled at 310 K. The pressure of the systems during aggregation is maintained at 1 bar in all directions; During the interaction between AuNP and lipid bilayer, the pressure within the plane of the bilayer is coupled controlled at 1 bar. The pressure along the out-of-plane direction is independently controlled at 1 bar. In such a way, the membrane tension in the simulation is guaranteed to be zero. Periodic boundary conditions are used in all of our simulations. The time step of all simulations is set as 30 fs. All simulations are performed using the Large-scale Atomic/Molecular Massively Parallel Simulator (LAMMPS) software⁶¹. The snapshots during the simulation process are rendered by the Visual Molecular Dynamics (VMD) software⁶².

3 Results and Discussion

3.1 pH-dependent stability of AuNPs

AuNPs show severe aggregation at moderate pH. The stability of the pH-responsive AuNPs is firstly investigated in our simulation. To study the aggregative or dispersed state of AuNPs in different pH environments, 27 AuNPs are initially evenly distributed in a simulation box of $(30 \times 30 \times 30) \text{ nm}^3$ at each pH value. Positively charged sodium or negatively charged chloride beads are added in each case to neutralize the simulation system. Each of the 27 AuNPs has been relaxed in a smaller simulation box of $(10 \times 10 \times 10) \text{ nm}^3$ for 100 ns before the aggregation simulation. Snapshots demonstrating the progression of AuNP state at pH values of $\text{pH} = 2.0, 5.3, 8.0$ are given in FigS.1 in the Support Information. As given in FigS.1, under the thermal fluctuation, each AuNP performs a random walk and has the chance to encounter and contact with each other. During this process, the AuNPs might be attractive or repulsive to each other, depending on their surface charge at different pH environments. The simulation of 27 AuNPs at each pH value lasts for 400 ns, beyond which the aggregative or dispersed state of NPs does not change. The relaxed structures of AuNPs are given in Fig.2 at each pH value. As we can see from the figure, the equilibrated state of the 27 AuNPs is critically affected by the pH value of environment. At $\text{pH} = 2.0$, due to the highly positive charged AuNP surfaces, these AuNPs are barely observed to contact or correlated with each other. Most of them are well dispersed in the simulation box. Similar well-dispersed states are observed at $\text{pH} = 3.0, 4.0$. All of these indicate that the AuNPs have good stability at low pH, despite the hydrophobic alkane chain. At the pH value of 4.5, around 20 percent of MUA

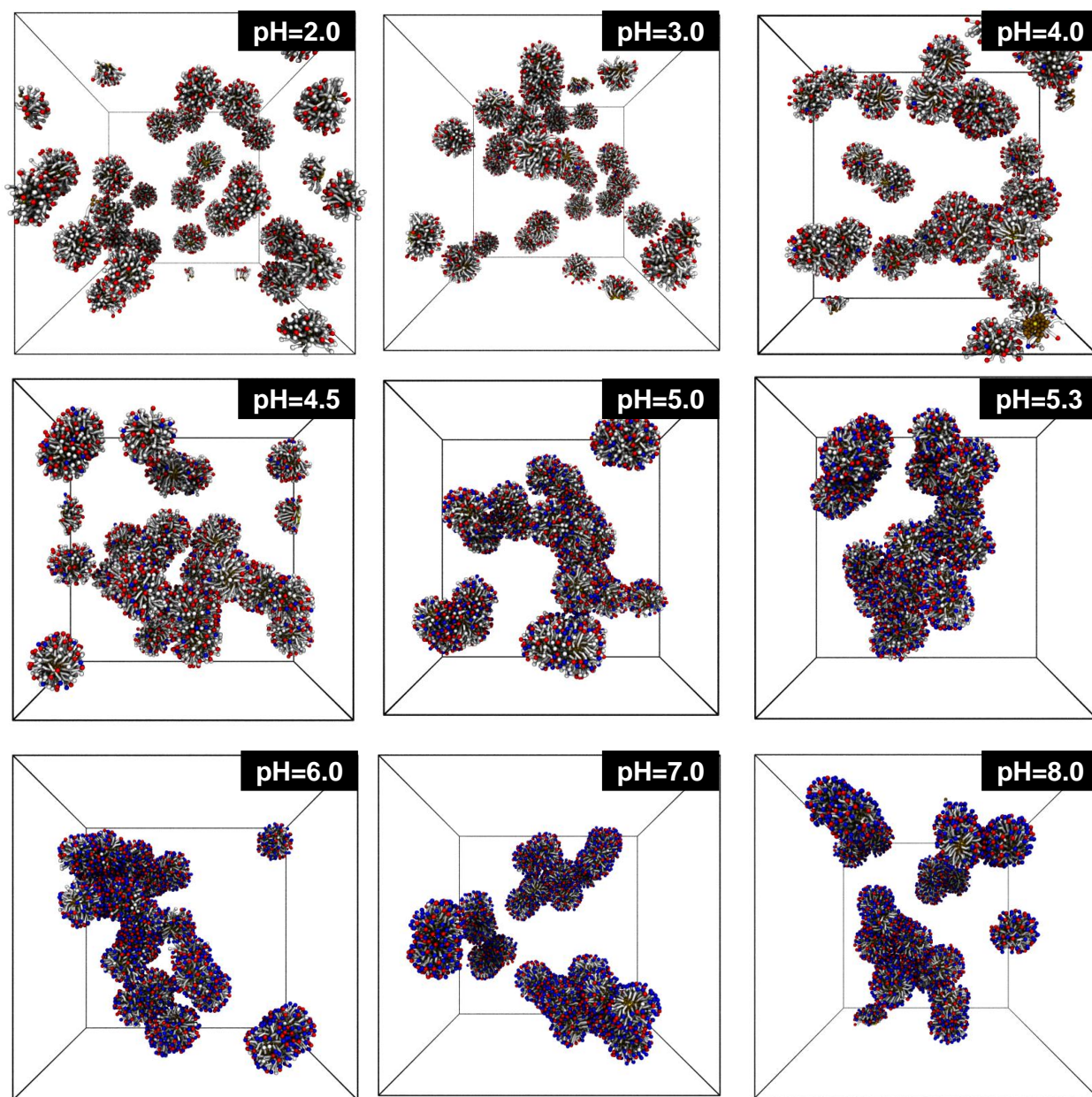


Fig. 2 Equilibrated state of 27 AuNPs at different pH environments. The water and ionic beads are not shown for clarity.

ligands are deprotonated, which is associated a dramatic decrease of positive net charge compared to $pH=2.0$ (cf. Fig. 1.C). Several AuNPs are observed connecting with each other to form a cluster at the state of equilibrium. This phenomenon is more pronounced at $pH=5.0$, where most of the AuNPs are correlated within their own clusters. These clusters do not increase their sizes with the simulation time, being dispersed in the simulation box instead of the individual AuNP. Furthermore, almost all of the AuNPs are correlated within one large cluster at the $pH=5.3$. This large cluster suggests severe aggregation of AuNPs at $pH=5.3$. It is also interesting to note that each AuNP has zero net charge at $pH=5.3$. As the increment of pH value, more MUA groups on the AuNPs are deprotonated, and each AuNP expresses overall negative charge in the system. At the pH values of 7.0 and 8.0, a similar state

to the one at $pH=5.0$ is observed: the small AuNPs clusters are dispersed in the simulation box. Note that these well dispersed small clusters are different from the large cluster at $pH=5.3$. These small clusters are stable in the simulation box and will not increase their size (cf. Fig.S3 in ESI[†]), which indicates that these AuNPs at high pH values can maintain their stability in solution. All of these simulation results indicate that the stability of AuNPs has the trend to recover with the increase of pH value.

To quantitatively characterize the aggregation behaviors of AuNPs, we calculate the radial distribution function (RDF) of the AuNPs and the corresponding second virial coefficient B_2 at different pH values. When calculating the RDF, only the COM of each AuNPs is considered to avoid the unreasonable peak caused by the FCC arrangement of Au beads. The RDF curve of each system is

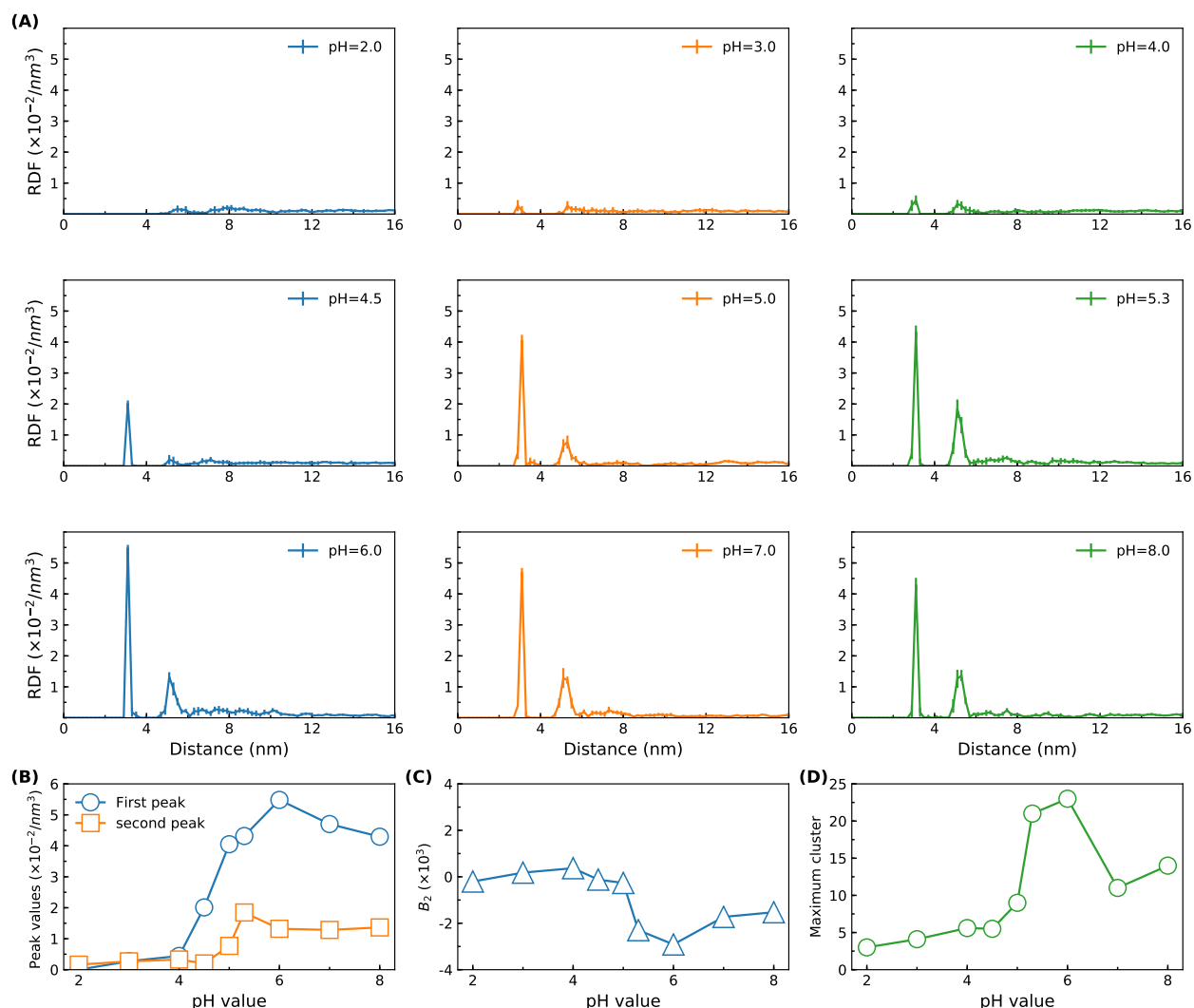


Fig. 3 Aggregation information about AuNPs at different pH values. (A) Radial distribution function (RDF) of AuNPs at different pH values. (B) The functions of the first and second peak values in RDF against the pH value. The first peak value for each pH value is the local maximum in the RDF curve at the distance around 3 nm. The second peak value for each pH value is the local maximum in the RDF curve at the distance around 5 nm. (C) The function of the B_2 value of the AuNPs against pH value. (D) The function of maximum cluster size against the pH value.

calculated by averaging 20 samples at their equilibrated states. As given in Fig.3, corresponding to the equilibrated state of AuNPs as shown in Fig.2, the RDF value of AuNPs is critically dependent on the pH environment. When $\text{pH} \leq 4.0$, there is no evident peak value in the RDF curves, which reflects the well-dispersed state of AuNPs. However, for the AuNPs at $\text{pH} \geq 4.5$, there are two pronounced peak values in RDF curves. The first peak appears at a distance around 3 nm, and the second peak is located at a distance around 5 nm. These two peak positions should be related to attractive interactions between ligands, which will be discussed in the free energy analysis. Furthermore, the value of the first peak is much larger than the second peak value. These two peak values in the RDF curves suggest that in the AuNP clusters observed in Fig.2, there are two different states corresponding to the COM distances of 3 nm and 5 nm. As we mentioned above, the diameter of the Au core is around 2.2 nm, and the diameter of a monolayer protected AuNP is around 5.5 nm. This indicates that

at the location of the first peak value, the AuNPs need to deform their ligands to interact and contact with each other.

To systematically compare the first and second peak values, we plot them against the pH values as shown in Fig.3.B. The first peak dramatically increases after $\text{pH}=4.0$ and reaches its maximum value at $\text{pH}=6.0$. After $\text{pH}=6.0$, it starts to decrease. A similar trend is observed for the second peak; while its maximum value occurs at $\text{pH}=5.3$. To more precisely quantify the AuNPs aggregated state, we calculate the B_2 based on the RDF curves according to the definition as $B_2 = -0.5 \int (g(r) - 1) 4\pi r^2 dr$, where $g(r)$ is the RDF of AuNPs. The B_2 value is a good indicator of the aggregation behavior of proteins and NPs⁶³⁻⁶⁵. A positive B_2 value indicates good dispersion of AuNPs, while a negative B_2 value suggests phase separation of AuNPs. As shown in Fig.3.C, the B_2 value of AuNPs dramatically decreases to negative values after $\text{pH} = 4.5$. However, it increases after $\text{pH} = 6.0$ with increment of pH value. To calibrate the cluster size in Fig.2, we further

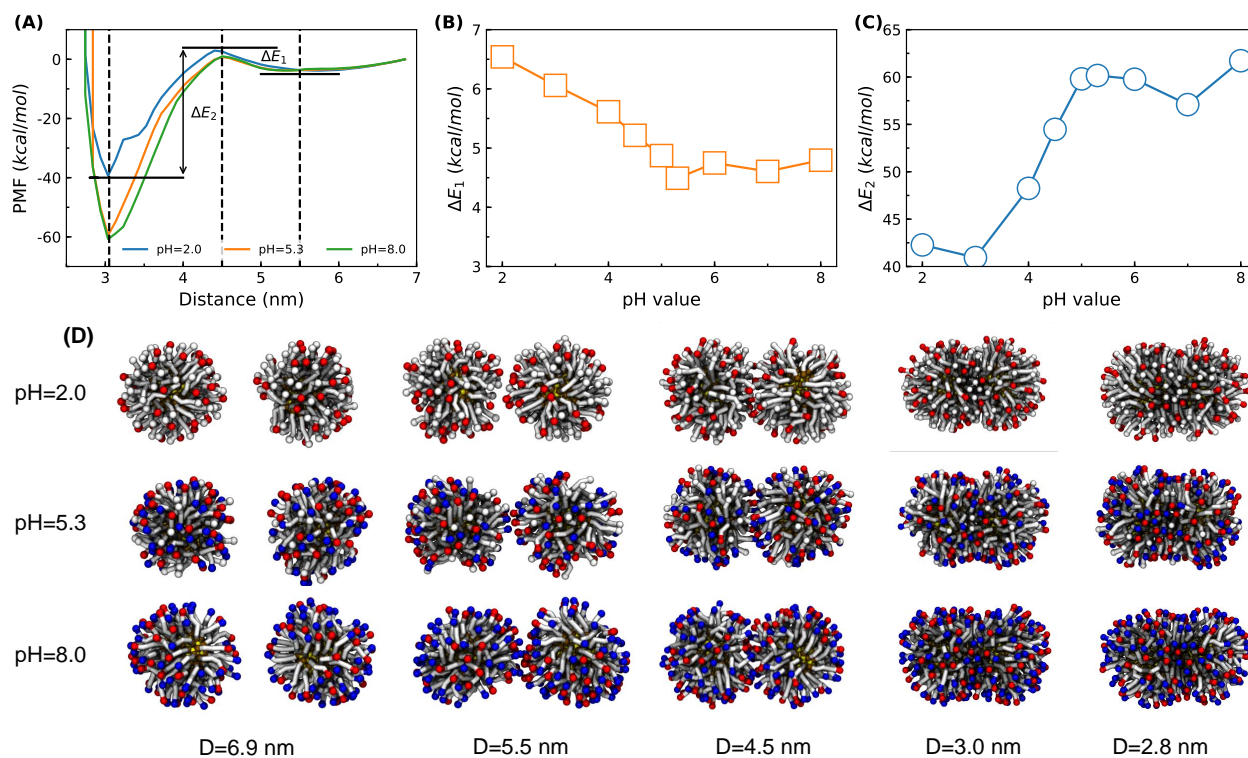


Fig. 4 Free energy analysis on aggregation of AuNPs. (A) The profile of potential of mean force (PMF) between two AuNPs against center-of-mass (COM) distance. (B) The change of energy barrier value to aggregate against pH values. (C) The change of energy barrier value to dissociate against pH values. (D) Configuration of AuNPs at different COM distances.

calculate the maximum cluster size in each system. AuNPs are considered to belong to a cluster if the COM distance between the AuNPs and any one within the cluster is smaller than 5.5 nm. As given in Fig.3.D, at the pH value of 5.3 and 6.0, maximum cluster size is significantly larger than the other pH. The cutoff distance will not affect the trend in these curves when counting the cluster size. As we can see, B_2 and maximum cluster size are consistent with each other. All of these indicate that around pH= 5.3, the AuNPs are severely aggregated. The AuNPs show well dispersed state at low pH and moderate dispersed at high pH. Our simulation results are consistent with those in experiments showing that the pH-responsive AuNPs are stable at both low and high pH²⁵. This typical characteristic of pH-responsive AuNPs can be utilized when designing smart NPs by choosing a suitable pKa value of functional groups according to the local pH environments in the blood flow and the tumor sites. It is also interesting to note that the larger size AuNPs have a better stability than the smaller ones at the same ligand grafting density as shown in Fig.S6 and Fig.S7 of the ESI†.

Free energy analysis reveals energy barrier before hydrophobic attraction. To reveal the physical mechanisms that determine the stability of AuNPs at different pH environments, we proceed to analyze the free energy change of two AuNPs approaching towards each other using the umbrella sampling method. This free energy change between the two AuNPs can reflect the interactive potential between them that determines the aggregation or dispersion of AuNPs in solution, as mentioned

above. During the analysis process, the two AuNPs are freely rotated to adjust their orientations. The potential of mean force (PMF) between two AuNPs are calculated against their COM distance. The PMF profile of AuNPs at the pH of 2.0, 5.3, and 8.0, and the corresponding configurations of AuNPs at different COM distances are given in Fig.4. PMF profiles for AuNPs at other pH values show similar trends. As we can tell from Fig.4.A, there are four typical regions found in the PMF profiles. At the initial COM distance around 7 nm, the AuNPs do not feel each other (cf.Fig.4.D). When they are approaching each other, there is a local minimum value in the PMF curve at a distance around 5.5 nm, which suggests the existence of an attractive force between AuNPs at this point. This attractive force should be associated with the second peak value in the RDF curves. Similar attraction is observed between two cationic NPs^{66,67}; this attraction is considered to be induced by an electrostatic bridging and a depletion-like force. For the mixed charged AuNPs, this attraction should also be caused by the electronic attraction between the functional groups. As shown in the configurations of AuNPs in Fig.4.D, at the distance of $D = 5.5$ nm for pH = 5.3 and pH = 8.0, the end groups in deprotonated negative MUA are attracted to the positive TMA end groups, which is reflected by the stretched ligand chain. When the two AuNPs are getting close to each other, there is a local maximum value around the distance of $D = 4.5$ nm. At this distance, the functional groups on the AuNPs begin to overlap with each other, a situation which might result in a large repulsive steric and electrostatic force. After $D = 4.5$ nm, the PMF

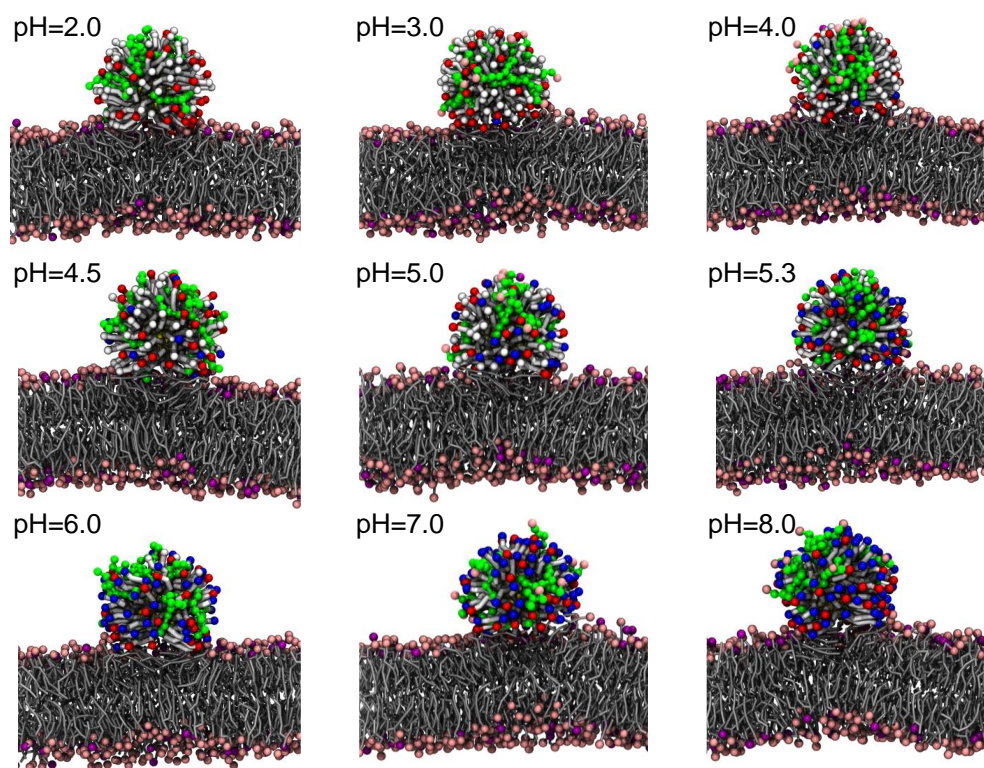


Fig. 5 Equilibrated snapshots of AuNPs adhering to lipid bilayers at different pH values. The head groups of DPPG are colored in pink, and the head groups of DPPC are colored in purple. The tails of lipids are colored in gray. The lipids extracted by the AuNPs are highlighted in green. The color scheme of the monolayer protected AuNP is the same as the one in Fig.1. All of the snapshots are obtained after a simulation time of 10 μ s.

between AuNPs dramatically decreases and reaches a global minimum at the distance of $D = 3.0$ nm. This global minimum is shown by the first peak position in the RDF curves and should be brought by the interaction between the hydrophobic chain as shown in the configurations in Fig.4.D. When the distance further decreases, the PMF instantly increases to a large positive value. Correspondingly, the ligands on AuNPs are highly overlapped.

The short ranged hydrophobic interaction is considered as a driving force for the aggregation of monolayer protected AuNPs³⁶. This hydrophobic driving force is also consistent with the global minimum in the PMF profile in our simulation. However, as we can see in the PMF profile, before the global minimum free energy state caused by the hydrophobic alkane chain, the AuNPs need to overcome an energy barrier between the local minimum at $D = 5.5$ nm and $D = 4.5$ nm. We mark this energy barrier as ΔE_1 . In addition, we mark the energy barrier between the local maximum at $D = 4.5$ nm and the global minimum at $D = 3.0$ nm as ΔE_2 . This energy difference height of ΔE_2 should be related to the dissociation ratio of AuNPs after they fall into the potential well at $D = 3.0$ nm. The variations of ΔE_1 and ΔE_2 against pH are plotted in Fig.4.B and Fig.4.C. As we can see in the figure, the energy barrier ΔE_1 decreases from the value of 6.5 kcal/mol at pH = 2.0 to the value around 4.5 kcal/mol at pH = 5.3. After pH = 5.3, the ΔE_1 slightly increases. On the other hand, the dissociation energy barrier ΔE_2 increases from the value of 42 kcal/mol at pH = 2.0 to the value around 60 kcal/mol at pH = 5.3. Then it

slightly changes against the pH value. It is interesting to note that all of the dissociation barriers ΔE_2 are larger than 40 kcal/mol, which is much larger than the thermal fluctuation. This indicates that for AuNPs at all pH values, they can hardly dissociate at the distance $D = 3.0$ nm, where the hydrophobic interaction plays the role. Therefore, a dispersed or aggregated state of AuNPs is determined by the value of energy barrier ΔE_1 . If ΔE_1 is larger than the energy obtained from thermal fluctuation, the AuNPs will be well dispersed. Otherwise, the AuNPs will aggregate together. To further confirm this hypothesis, we calculate the transnational kinetic energy distribution of a single AuNPs at $T = 310$ K. As given in Fig.S5, the mean transnational kinetic energy of an AuNPs is round 0.93 kcal/mol. And the largest transnational kinetic energy during the testing time (300 ns) is 3.67 kcal/mol with a probability of 2×10^{-4} . Comparing the values of transnational kinetic energy and energy barrier ΔE_1 , we can get that $\Delta E_1 = 6.5$ kcal/mol at pH = 2.0 is large enough to prevent the AuNPs aggregate together. On other other hand, the value of $\Delta E_1 = 4.5$ kcal/mol is comparable to the largest transnational kinetic energy, resulting the aggregation of AuNPs at pH = 5.3. To the best of our knowledge, this is the first time, it has been clarified using simulation that the energy barrier before the hydrophobic attraction is crucial to the stability of monolayer protected AuNPs in solution.

As indicated by the B_2 and maximum cluster size, the stability of AuNPs starts to recover at pH = 7.0 and pH = 8.0. In comparison, their ΔE_1 and ΔE_2 are similar to the ones at pH = 5.3 and

pH = 6.0. We hypothesize that this is caused by the angular dependence of the PMF profiles due to the random distribution of ligands on AuNP surface. Note that during the umbrella sampling process, the AuNPs are free to rotate to search the minimal energy at each COM position. The similarity in ΔE_1 and ΔE_2 suggests that the AuNPs at pH = 7.0 and pH = 8.0 are able to associate with each other at certain relative angular position. But at other certain relative angular positions, the ΔE_1 and ΔE_2 might be different. To confirm this, we perform the umbrella sampling process of two AuNPs at pH = 7.0 and pH = 8.0 with a fixed relative orientation. As given in Fig.S4 of the ESI†, with the fixed relative orientation, the ΔE_1 values at pH = 7.0 and pH = 8.0 increase to 5.7 kcal/mol and 5.8 kcal/mol, respectively, which are comparable to the one (6.0 kcal/mol) at pH = 3.0. The combination of PMF profiles with free rotation and fixed rotation should be able to explain the phenomena that at high pH values, the AuNPs form small clusters. But these small clusters are stable and will not increase their size.

3.2 pH-independent adhesion of AuNPs on lipid bilayer

AuNPs adhere on lipid bilayer at all pH values. After clarifying the aggregation behavior of AuNPs at different pH environments, we proceed to study the interaction between AuNPs and lipid bilayers. In this part, the AuNPs at different pH values are initially placed above the lipid bilayers with a distance of 7 nm. The lipid bilayers in all of these cases have the same composition of DPPG:DPPC = 5 : 1. Sodium beads are added in each case to neutralize the simulation system. We run these simulations for more than 10 μ s. It is interesting to find that none of the AuNPs can insert into the bilayers at all pH values, as shown in the equilibrated state of each system in Fig.5. Instead, all of the AuNPs show preference to adhere onto the bilayer surface, due to the attraction between the positive charged TMA ends and the negative charged lipid bilayers. Furthermore, as marked in Fig.5, the lipids in the bilayer are observed to be extracted by the adhering AuNPs. These extracted lipids climb up onto the AuNPs surface. It is also noteworthy that even at the high pH values (pH = 7.0, 8.0) where the AuNPs have net negative charge, they still show adhesion on the lipid bilayer and extraction of lipid molecules after adhering. Our results seem to conflict with those done by Lin et.al⁴⁹ showing that the monolayer-protected AuNPs have the chance to penetrate into the lipid bilayer, which is highly dependent on the surface charge of AuNPs. However, different from the AuNPs studied by Lin et.al, all the hydrophobic alkane chains here, are modified with hydrophilic functional groups on the pH-responsive AuNPs. The penetration process of monolayer protected AuNPs is reported to be a balance between the hydrophobic driving force and the energy cost to snorkeling the functional end groups^{46,68}. With the hydrophilic ends, snorkeling of the end groups might require a large energy penalty. To further confirm this, we investigate all-TMA and no-MUA AuNPs interacting with lipid bilayer. The surface of all-TMA AuNP is only decorated with TMA ligands. Comparing with the pH-responsive AuNPs, the MUA ligands are replaced by the pure hydrophobic alkane chains on the no-MUA AuNP. The setting of no-MUA AuNP is similar to the one

in Ref.⁴⁷. As we can in Fig.S8 of ESI†, though the all-TMA AuNP has a larger surface charge, it adheres on the lipid bilayer over the entire simulation time. However, the no-MUA AuNP quickly penetrates into the lipid bilayer. Further free energy analysis for penetration will be revealed in the following section. On the other hand, the extraction of lipids has interesting implications. It has been shown that the extraction of lipids by nanomaterials such as graphene⁶⁹ might be destructive to the cell membrane. This information might indicate another destructive mechanism for the charged AuNPs other than the direct pore opening on the cell membrane⁴⁹. In addition, the lipid extraction might be able to explain the dehydration of lipid bilayers⁴⁴ even when the AuNPs are not inserted into the bilayer. We will discuss the membrane destruction and dehydration in the following part. We should also emphasize that the mixed-charged AuNPs in previous experimental studies²⁵ are much larger than the ones considered in present simulations. In addition, serum proteins exist during the cellular uptake process. These serum proteins decorated large size AuNPs (> 5 nm) might be internalized by the endocytosis pathways¹⁵. While the small size proteins free AuNPs (< 5 nm) could penetrate into lipid bilayer under certain conditions⁴⁹.

Extraction of lipids show a protrusion and climbing up process. To reveal the details about this adhesion and lipid extraction process, we show the snapshots of this interactive process with highly positive and negative charge AuNPs at the pH values of 2.0 and 8.0, respectively. As given in Fig.5.A for pH = 2.0, the AuNP is initially placed above the lipid bilayer at a distance of $D \approx 7$ nm. Because of the attraction between the positively charged TMA on AuNP and the negatively charged DPPG head group, the AuNP quickly adheres onto the lipid bilayer. Furthermore, driven by the hydrophobic attraction between the alkane chain in the TMA/MUA ligands and the lipid tails, the ligands on the AuNP surface deform and the lipids in the bilayer rearrange themselves, which result in a hydrophobic contact area between the AuNP and the lipid bilayer ($t = 0.15 \mu$ s in Fig.5.A for pH = 2.0). As we can tell in the snapshot, the lipids near the contact region are highly disordered. These disordered lipid molecules are supposed to promote the lipid protrusion that helps the insertion of AuNP into the lipid bilayer⁴⁸. Interestingly, as highlighted at $t = 0.16 \mu$ s, one lipid protrudes with a tail group that remains interacting with the lipids in the bilayer. While, the other tail group starts to insert into the hydrophobic part of ligands on the AuNP. The lipid molecule protrudes and splays between the AuNPs and lipid bilayer. Afterwards, rather than help the insertion of AuNPs as reported in Ref⁴⁸, the protruded lipid molecule quickly climbs up on to the AuNPs surface, with its two tail groups splay and are embedded in the hydrophobic part of the ligand, and its head group points towards the outside of AuNP surface. After a long period of 10 μ s, there are almost 10 lipid molecules extracted by the adhering AuNPs following the same protruding and climbing up process. Moreover, though the AuNP at high pH value of 8.0 possesses highly negatively charge, a similar process is observed. This might suggest that the local charge distribution of the monolayer-protected AuNPs, rather than the net charge, is more important to the adhesion of AuNPs on cell membranes. We further monitor the evolution of extracted lipid number on AuNPs

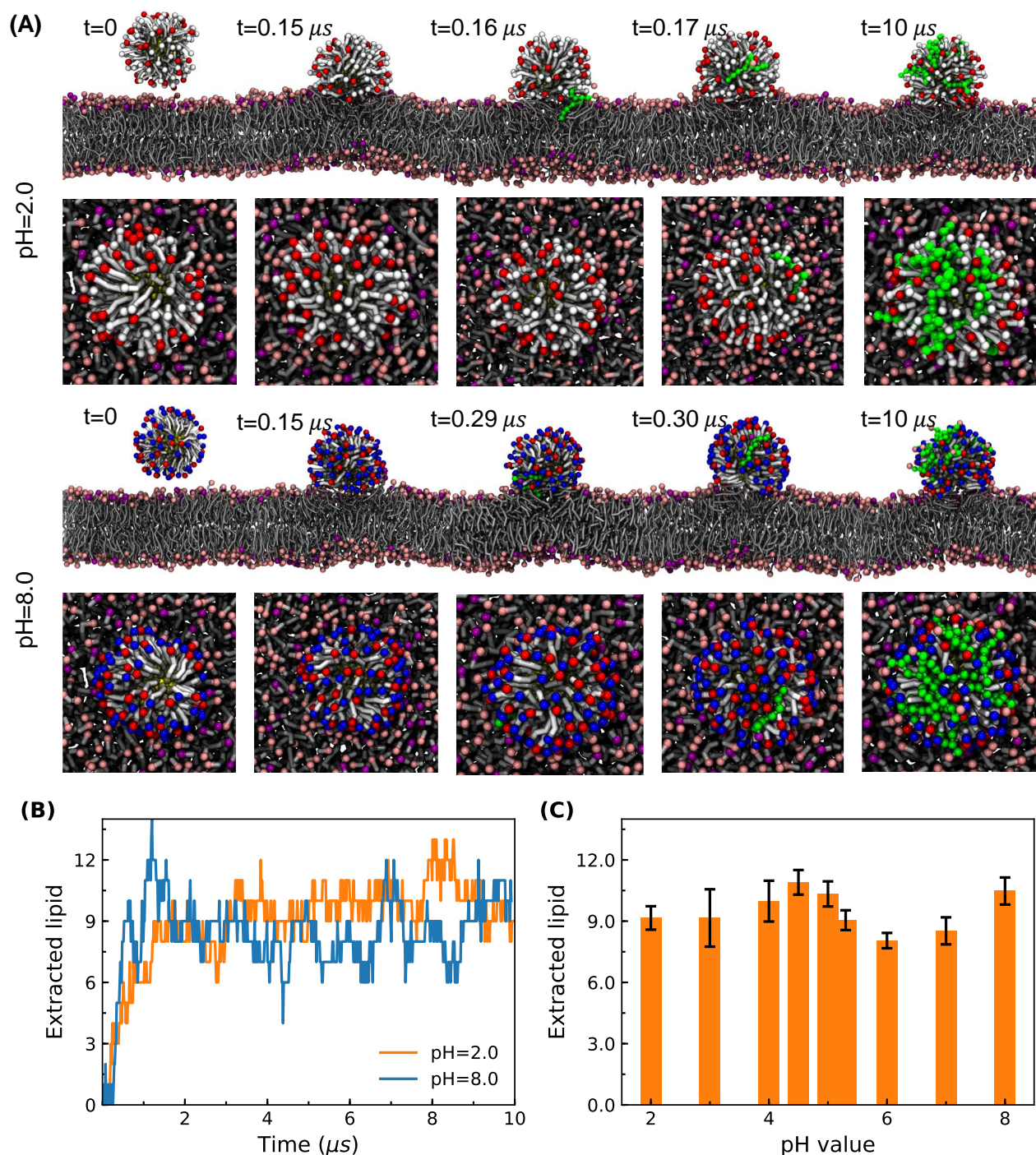


Fig. 6 (A) Adhesion process of AuNPs at pH = 2.0 and pH = 8.0 onto the lipid bilayer. The lipids marked in green are those extracted by the AuNPs. (B) Number of AuNP-extracted lipids over simulation time at pH = 2.0 and pH = 8.0. (C) The number of AuNP-extracted lipids at different pH values.

of pH = 2.0 and pH = 8.0 as shown in Fig.6.B. It is interesting to note that in both cases, the number of extracted lipids increases dramatically at the early state ($t < 2 \mu s$) and then saturates at the later state. It is also noteworthy that the extracted lipids still have the chance to return back to the lipid bilayer, as we can tell from the fluctuation of the extracted lipid number. We also calculate the extracted lipid numbers of AuNPs at different pH values as given in Fig.6.C. The extracted lipid number of other cases

is around 10. This saturated lipid number might be affected by the AuNPs size and the length of ligands, which can be manipulated when designing the surface functionalization of AuNP. Note that the extraction of lipids has also been observed by Van Lehn and Alexander-Katz⁷⁰ after the insertion of AuNPs into bilayers, which indicates that lipid extraction might be a common behavior of charged monolayer protected AuNPs interacting with cell membrane.

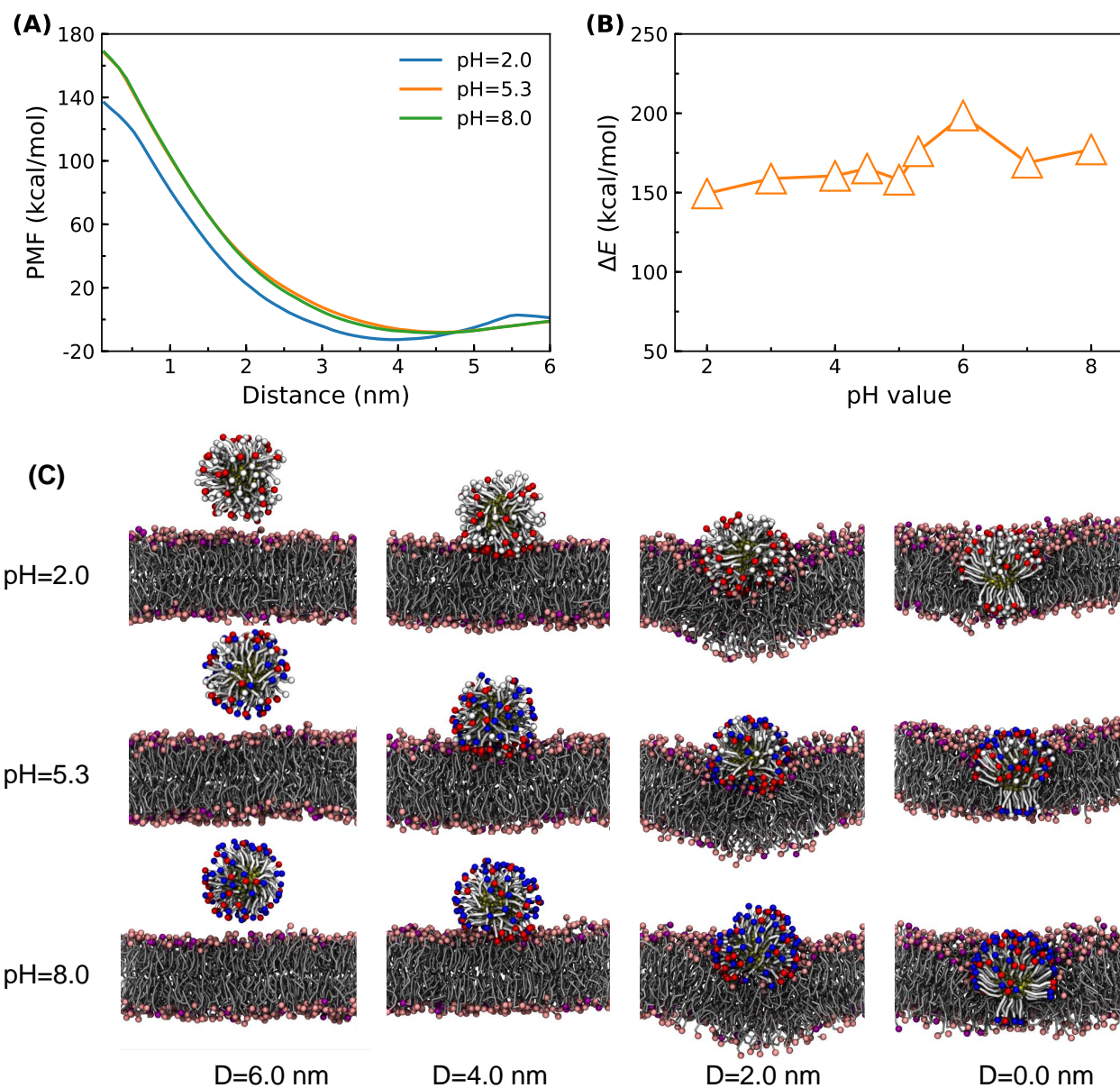


Fig. 7 Free energy analysis for AuNP penetration into lipid bilayer. (A) The PMF profile of directing an AuNP to penetrate into a lipid bilayer. The three curves represent the AuNPs at the pH values of 2.0, 5.3 and 8.0. (B) The variation of energy barrier ΔE during penetration process for different pH values. ΔE denotes the energy difference between the global minimum and maximum values in (A). (C) Configurations of AuNPs and lipid bilayer during penetration process at different pH values.

Free energy analysis reveals large energy barriers associated with AuNP penetration. To understand why the pH-responsive AuNPs are adhering onto rather than penetrating into the bilayer, we perform a series of simulations to analyze the free energy change when inserting the AuNP into the bilayer. This penetration process is directed by a spring potential as mentioned in the corresponding section of the description of methods. As shown in Fig.7.A of the PMF profile, this penetration process can be divided into two regions. Before the COM distance of $D = 4.0$ nm, due to the attraction between positive charge TMA and negative DPPG head group as we can see in Fig.7.C at $D = 4.0$ nm, the free energy decreases a small amount to a global minimum value. When the AuNPs and lipid bilayer further approach each other,

the PMF values dramatically increase. Within this COM distance region, though the hydrophobic interaction between the alkane chain and lipid tail is preferred, due to the energy barrier induced by the hydrophilic functional group, the ligand on the AuNPs surfaces can hardly translocate through the hydrophobic part of lipid bilayer and reach the other side of the bilayer. Instead, the ligands on the AuNPs largely deform to squeeze each other, which is combined with the highly curved lipid bilayers as shown in Fig.7.C at $D = 2.0$ nm. The PMF value further increases, even if the ligands on AuNPs snorkels and the AuNP is translocated through the lipid bilayer. As we can tell in Fig.7.C at $D = 0.0$ nm, the snorkeling of ligands causes great stretching of the ligand chains, which indicates that the large steric interaction might lead to this high

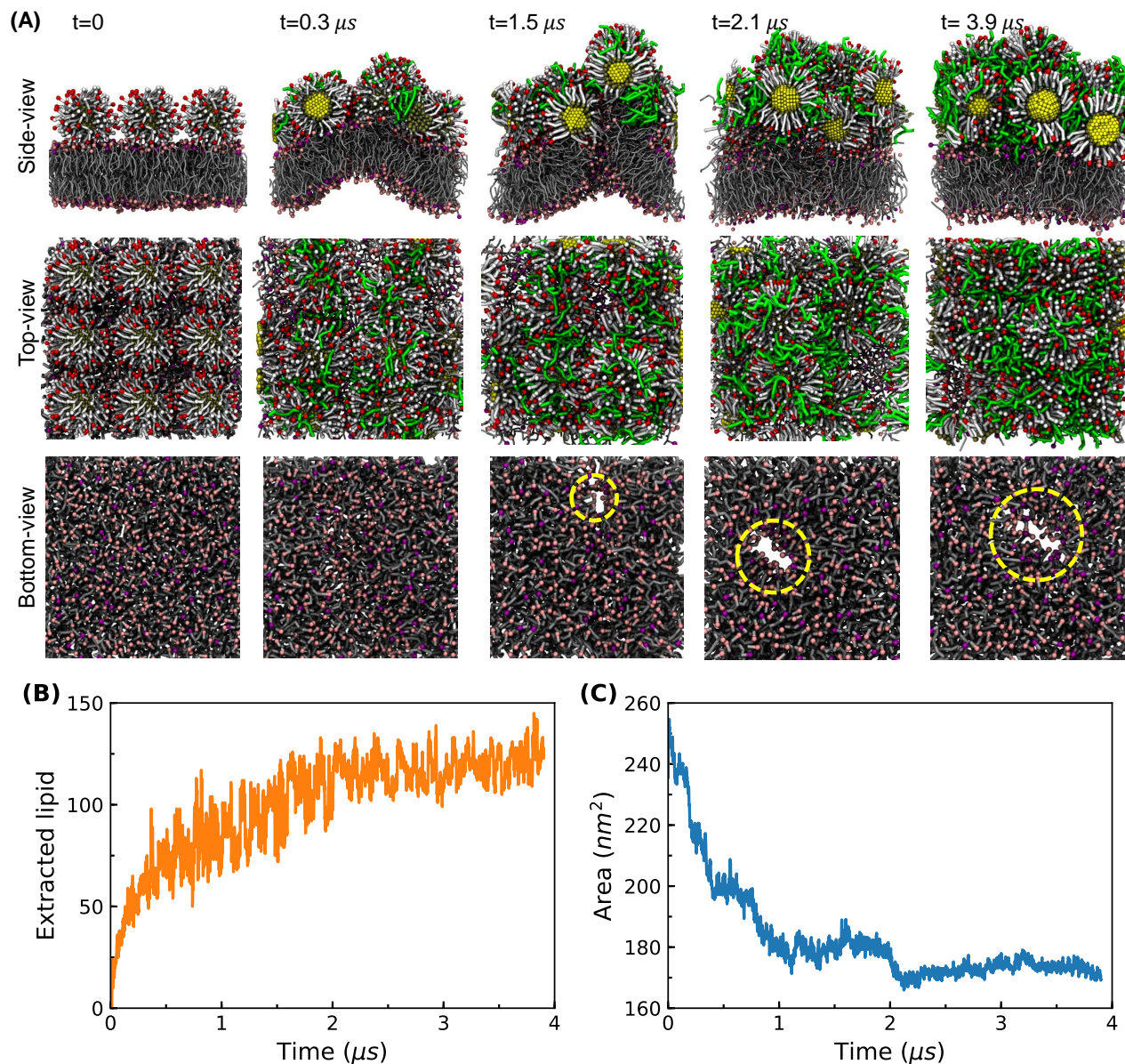


Fig. 8 Interaction between multiple AuNPs and model lipid bilayer. (A) Snapshots of interaction process between multiple AuNPs and lipid bilayer. The lipids extracted by AuNPs are highlighted in green. A pore opened in lipid bilayer is highlighted by circles. (B) Number of extracted lipids over simulation time. (C) Evolution of the lipid bilayer area. The pH value in the system is 2.0.

energy state when the AuNPs are inserted into the lipid bilayer. A similar PMF profile is observed by Chen et.al.⁷¹, when most of the ligand is functionalized with anionic groups. The PMF profiles of AuNPs at different pH values are similar. Only a slight shift in the PMF value is observed, due to the existence of negatively charged (or deprotonated) MUA. To evaluate the energy cost of inserting the AuNPs into the bilayer, we calculate the free energy difference between the global minimum and maximum in the PMF profile and name it as ΔE . As we can see in Fig.7.B, due to the increased deprotonated MUA at higher pH value, the ΔE increases with the pH value. However, it is more important to note that the energy cost of ΔE in all cases is larger than 150 kcal/mol, which is much larger than the thermal fluctuation. This energy cost ΔE for AuNPs with all alkane chains functionalized

with hydrophilic end groups is totally different from the ones with negative and hydrophobic ligands in Ref^{46,47}. When a part of the ligand is an alkane chain without a functional group, the free energy decreases around 100 kcal/mol for the favorable hydrophobic interaction^{46,47}. This indicates that it is thermodynamically unfavorable to insert the pH-responsive AuNPs into the lipid bilayer when all the alkane chains are functionalized. This is further confirmed by the comparison of PMF profiles between different AuNPs at pH= 2.0: mixed charged AuNPs, all-TMA AuNP and no-MUA AuNPs as given in Fig.S9 of ESI[†]. Disordered lipid membrane region and longer alkane chain length might be desirable, if the penetration of pH-responsive AuNPs is preferred^{46,71}.

Interaction between multiple AuNPs and model lipid bilayer. To test our hypothesis about the relation between lipid

extraction and membrane disruption/dehydration, we proceed to investigate the interaction between multiple AuNPs and model lipid bilayer. The pH value of system here is $\text{pH} = 2.0$. As given in Fig.8.A, 9 monolayer-protected AuNPs are placed above the lipid bilayer at $t = 0$. Similar to the adhesion process of single AuNP, all the AuNPs are adhered on the lipid bilayer at $t = 0.3 \mu\text{s}$. At the same time, many lipids are extracted by these AuNPs, which causes the wrinkle of bilayer. At $t = 1.5 \mu\text{s}$, the AuNPs adjust their position on the bilayer. With more lipids extracted, a small pore opens in the bilayer. This pore does not expand much at $t = 2.1 \mu\text{s}$ and $t = 3.9 \mu\text{s}$, when the AuNPs are almost covered by the extracted lipids. We further calculate the number of extracted lipids and the area of lipid bilayer in Fig.8.B, and Fig.8.C respectively. As we can tell, the extracted lipid number increases up to 140. With the extraction of lipids in bilayer, the bilayer area significantly decreases from 260 nm^2 to 170 nm^2 . To avoid the potential influence of small membrane size on the lipid extraction and dehydration, we further perform simulations of a larger membrane with initial area of 1225 nm^2 . As given in Fig.S10 and Fig.S11 of ESI†, two different AuNP numbers, 36 and 25, are studied, similar lipid extraction and bilayer dehydration are observed. Our results confirm that the adhesion of multiple AuNPs can significantly increase the extracted lipid number and lead to the dehydration of lipid bilayer. Furthermore, the pore induced by extracted lipids provides another possible mechanism about cell membrane disruption, apart from the penetration induced pore opening⁴⁹. Note that the similar phenomena have been observed at other pH values in our simulations (results not shown here).

4 Conclusions

In this work, we have systematically investigated the stability and cellular interaction of pH-responsive monolayer protected AuNPs through CG molecular dynamics simulations. The AuNPs in our simulations are decorated with positively charged TMA ligands and MUA ligands with $\text{pK}_a = 5.08$. Therefore, MUA ligands are protonated and neutral at low pH (< 5.3) and deprotonated and negatively charged at high pH (> 5.3). All of these factors combined together make the AuNPs pH-responsive. The monolayer protected AuNPs are positively charged at low pH and possess negative overall charge at high pH. Our simulation results suggest that the pH-responsive AuNPs are severely aggregated at a moderate pH value around 5.3, and they are stable and dispersed at both low and high pH. The RDF of AuNPs indicates that there are two peak values at the RDF curves, which correspond to COM distances around 5.5 nm and 3.0 nm , respectively. These two peak values suggest two different correlated states within the aggregated cluster. Furthermore, we perform the free energy analysis of two AuNPs to understand free energy barriers associated with AuNPs aggregation. We found that the first peak at $D = 3.0 \text{ nm}$ is induced by the hydrophobic driving force between alkane chain of ligands, while the second peak at $D = 5.5 \text{ nm}$ is caused by the electrostatic bridging between two mixed charged AuNPs. More importantly, it is found that the energy barrier between $D = 5.5 \text{ nm}$ and $D = 3.0 \text{ nm}$ is the key that determines the stability of monolayer-protected AuNPs at different pH values. This energy barrier is dramatically decreased at

moderate pH values, which contributes to the severe aggregation of AuNPs. We further investigate the interaction between AuNPs and lipid bilayers; it is interesting to find that all AuNPs adhere onto the lipid bilayer, independent of their surface charges. Moreover, the lipids originally in the bilayer are extracted by the AuNPs through a protrusion process. This extraction of lipids will result in dehydration and disruption of bilayers, if multiple AuNPs exist. Further free energy analysis reveals that the penetration of AuNPs will lead to dramatic free energy increase because of deformation of ligands and hydrophilic functional end groups. Our simulations for the first time systematically study the stability of pH-responsive AuNPs and their interaction with lipid bilayers in simulation, which might help the design of pH-responsive monolayer protected AuNPs.

Conflicts of interest

There are no conflicts to declare.

Acknowledgments

We would like to thank the support from National Science Foundation (REU-1560098). Z.S., H.Y. and Y.L. are grateful for support from the Department of Mechanical Engineering at the University of Connecticut. Z.S. and H.Y. would like to thank the GE Fellowship for Innovation for partial financial support. This research benefited from the computational resources and staff contributions provided by the Booth Engineering Center for Advanced Technology (BECAT) at the University of Connecticut. Part of this work used the Extreme Science and Engineering Discovery Environment (XSEDE), which is supported by the National Science Foundation grant number ACI-1053575.

References

- 1 S. Rana, A. Bajaj, R. Mout and V. M. Rotello, *Adv. Drug Delivery Rev.*, 2012, **64**, 200–216.
- 2 J. D. Gibson, B. P. Khanal and E. R. Zubarev, *J. Am. Chem. Soc.*, 2007, **129**, 11653–11661.
- 3 X. Sun, G. Zhang, R. S. Keynton, M. G. O’Toole, D. Patel and A. M. Gobin, *Nanomed. Nanotechnol. Biol. Med.*, 2013, **9**, 1214–1222.
- 4 Y.-S. Yang, R. P. Carney, F. Stellacci and D. J. Irvine, *ACS Nano*, 2014, **8**, 8992–9002.
- 5 R. Xiong, K. Raemdonck, K. Peynshaert, I. Lentacker, I. De Cock, J. Demeester, S. C. De Smedt, A. G. Skirtach and K. Braeckmans, *ACS Nano*, 2014, **8**, 6288–6296.
- 6 E. Boisselier and D. Astruc, *Chem. Soc. Rev.*, 2009, **38**, 1759–1782.
- 7 E. C. Dreaden, A. M. Alkilany, X. Huang, C. J. Murphy and M. A. El-Sayed, *Chem. Soc. Rev.*, 2012, **41**, 2740–2779.
- 8 L. C. Kennedy, L. R. Bickford, N. A. Lewinski, A. J. Coughlin, Y. Hu, E. S. Day, J. L. West and R. A. Drezek, *Small*, 2011, **7**, 169–183.
- 9 E. C. Dreaden, M. A. Mackey, X. Huang, B. Kang and M. A. El-Sayed, *Chem. Soc. Rev.*, 2011, **40**, 3391–3404.
- 10 H. Häkkinen, *Nat. Chem.*, 2012, **4**, 443.

- 11 H. Maeda, T. Sawa and T. Konno, *J. Controlled Release*, 2001, **74**, 47–61.
- 12 W. C. Chan, *Acc. Chem. Res.*, 2017, **50**, 627–632.
- 13 S. Wilhelm, A. J. Tavares, Q. Dai, S. Ohta, J. Audet, H. F. Dvorak and W. C. Chan, *NAT REV MATER*, 2016, **1**, 16014.
- 14 Z. Shen, M.-P. Nieh and Y. Li, *Polymers*, 2016, **8**, 83.
- 15 A. Albanese, P. S. Tang and W. C. Chan, *Annu. Rev. Biomed. Eng.*, 2012, **14**, 1–16.
- 16 Q. Dai, S. Wilhelm, D. Ding, A. M. Syed, S. Sindhwani, Y. Zhang, Y. Y. Chen, P. MacMillan and W. C. Chan, *ACS nano*, 2018, **12**, 8423–8435.
- 17 Y. Li, X. Li, Z. Li and H. Gao, *Nanoscale*, 2012, **4**, 3768–3775.
- 18 Y. Nademi, T. Tang and H. Uludağ, *Nanoscale*, 2018, **10**, 17671–17682.
- 19 W. Gao, J. M. Chan and O. C. Farokhzad, *Mol. Pharmaceutics*, 2010, **7**, 1913–1920.
- 20 S. Wang, P. Huang and X. Chen, *ACS Nano*, 2016, **10**, 2991–2994.
- 21 L. Y. Chou, K. Zagorovsky and W. C. Chan, *Nature nanotechnology*, 2014, **9**, 148–155.
- 22 H. Cheng, J.-Y. Zhu, X.-D. Xu, W.-X. Qiu, Q. Lei, K. Han, Y.-J. Cheng and X.-Z. Zhang, *ACS Appl. Mater. Interfaces*, 2015, **7**, 16061–16069.
- 23 L. E. Gerweck and K. Seetharaman, *Cancer Res.*, 1996, **56**, 1194–1198.
- 24 K. Saha, S. S. Agasti, C. Kim, X. Li and V. M. Rotello, *Chemical reviews*, 2012, **112**, 2739–2779.
- 25 P. P. Pillai, S. Huda, B. Kowalczyk and B. A. Grzybowski, *J. Am. Chem. Soc.*, 2013, **135**, 6392–6395.
- 26 X. Liu, H. Huang, Q. Jin and J. Ji, *Langmuir*, 2011, **27**, 5242–5251.
- 27 P. J. Bonitatibus Jr, A. S. Torres, B. Kandapallil, B. D. Lee, G. D. Goddard, R. E. Colborn and M. E. Marino, *ACS Nano*, 2012, **6**, 6650–6658.
- 28 X. Liu, Q. Jin, Y. Ji and J. Ji, *J. Mater. Chem.*, 2012, **22**, 1916–1927.
- 29 R. C. Murdock, L. Braydich-Stolle, A. M. Schrand, J. J. Schlager and S. M. Hussain, *Toxicol. Sci.*, 2008, **101**, 239–253.
- 30 G. Maiorano, S. Sabella, B. Sorce, V. Brunetti, M. A. Malvindi, R. Cingolani and P. P. Pompa, *ACS Nano*, 2010, **4**, 7481–7491.
- 31 A. Albanese and W. C. Chan, *ACS Nano*, 2011, **5**, 5478–5489.
- 32 A. M. Kalsin, B. Kowalczyk, S. K. Smoukov, R. Klajn and B. A. Grzybowski, *J. Am. Chem. Soc.*, 2006, **128**, 15046–15047.
- 33 K. J. Bishop and B. A. Grzybowski, *ChemPhysChem*, 2007, **8**, 2171–2176.
- 34 G. A. DeVries, M. Brunnbauer, Y. Hu, A. M. Jackson, B. Long, B. T. Neltner, O. Uzun, B. H. Wunsch and F. Stellacci, *Science*, 2007, **315**, 358–361.
- 35 O. Uzun, Y. Hu, A. Verma, S. Chen, A. Centrone and F. Stellacci, *Chem. Commun.*, 2008, 196–198.
- 36 R. C. Van Lehn and A. Alexander-Katz, *Langmuir*, 2013, **29**, 8788–8798.
- 37 J. Zhou, J. Ralston, R. Sedev and D. A. Beattie, *J. Colloid Interface Sci.*, 2009, **331**, 251–262.
- 38 T. Kim, C.-H. Lee, S.-W. Joo and K. Lee, *J. Colloid Interface Sci.*, 2008, **318**, 238–243.
- 39 J.-Q. Lin, H.-W. Zhang, Z. Chen, Y.-G. Zheng, Z.-Q. Zhang and H.-F. Ye, *J. Phys. Chem. C*, 2011, **115**, 18991–18998.
- 40 S. Wang, Z. Teng, P. Huang, D. Liu, Y. Liu, Y. Tian, J. Sun, Y. Li, H. Ju, X. Chen *et al.*, *Small*, 2015, **11**, 1801–1810.
- 41 D. L. Thorek and A. Tsourkas, *Biomaterials*, 2008, **29**, 3583–3590.
- 42 I. Slowing, B. G. Trewyn and V. S.-Y. Lin, *J. Am. Chem. Soc.*, 2006, **128**, 14792–14793.
- 43 P. R. Leroueil, S. A. Berry, K. Duthie, G. Han, V. M. Rotello, D. Q. McNerny, J. R. Baker, B. G. Orr and M. M. Banaszak Holl, *Nano Lett.*, 2008, **8**, 420–424.
- 44 S. Tatur, M. Maccarini, R. Barker, A. Nelson and G. Fragneto, *Langmuir*, 2013, **29**, 6606–6614.
- 45 C. M. Goodman, C. D. McCusker, T. Yilmaz and V. M. Rotello, *Bioconjugate Chem.*, 2004, **15**, 897–900.
- 46 R. C. Van Lehn and A. Alexander-Katz, *Soft Matter*, 2014, **10**, 648–658.
- 47 R. C. Van Lehn, P. U. Atukorale, R. P. Carney, Y.-S. Yang, F. Stellacci, D. J. Irvine and A. Alexander-Katz, *Nano Lett.*, 2013, **13**, 4060–4067.
- 48 R. C. Van Lehn, M. Ricci, P. H. Silva, P. Andreozzi, J. Reguera, K. Voitchovsky, F. Stellacci and A. Alexander-Katz, *Nat. Commun.*, 2014, **5**, 4482.
- 49 J. Lin, H. Zhang, Z. Chen and Y. Zheng, *ACS Nano*, 2010, **4**, 5421–5429.
- 50 S. J. Marrink, A. H. De Vries and A. E. Mark, *J. Phys. Chem. B*, 2004, **108**, 750–760.
- 51 S. J. Marrink, H. J. Risselada, S. Yefimov, D. P. Tieleman and A. H. De Vries, *J. Phys. Chem. B*, 2007, **111**, 7812–7824.
- 52 H. J. Risselada and S. J. Marrink, *Proc. Natl. Acad. Sci. U.S.A.*, 2008, **105**, 17367–17372.
- 53 V. Corradi, E. Mendez-Villuendas, H. I. Ingolfsson, R.-X. Gu, I. Siuda, M. N. Melo, A. Moussatova, L. J. DeGagne, B. I. Sejdju, G. Singh *et al.*, *ACS Cent. Sci.*, 2018, **4**, 709–717.
- 54 F. Grunewald, G. Rossi, A. H. De Vries, S. J. Marrink and L. Monticelli, *J. Phys. Chem. B*, 2018, **122**, 7436–7449.
- 55 J. Lin, H. Zhang, V. Morovati and R. Dargazany, *J. Colloid Interface Sci.*, 2017, **504**, 325–333.
- 56 H. Sharma and E. E. Dormidontova, *ACS Nano*, 2017, **11**, 3651–3661.
- 57 A. Adnan, R. Lam, H. Chen, J. Lee, D. J. Schaffer, A. S. Barnard, G. C. Schatz, D. Ho and W. K. Liu, *Molecular pharmaceutics*, 2011, **8**, 368–374.
- 58 F. Simonelli, D. Bochicchio, R. Ferrando and G. Rossi, *J. Phys. Chem. Lett.*, 2015, **6**, 3175–3179.
- 59 G. M. Torrie and J. P. Valleau, *J. Comput. Phys.*, 1977, **23**, 187–199.
- 60 S. Kumar, J. M. Rosenberg, D. Bouzida, R. H. Swendsen and P. A. Kollman, *J. Comput. Chem.*, 1992, **13**, 1011–1021.
- 61 S. Plimpton, *J. Comput. Phys.*, 1995, **117**, 1–19.

- 62 W. Humphrey, A. Dalke and K. Schulten, *J. Mol. Graphics*, 1996, **14**, 33–38.
- 63 L. J. Quang, S. I. Sandler and A. M. Lenhoff, *J. Chem. Theory Comput.*, 2014, **10**, 835–845.
- 64 A. Grunberger, P.-K. Lai, M. A. Blanco and C. J. Roberts, *J. Phys. Chem. B*, 2013, **117**, 763–770.
- 65 G. Hou, W. Tao, J. Liu, Y. Gao, L. Zhang and Y. Li, *Physical Chemistry Chemical Physics*, 2017, **19**, 32024–32037.
- 66 G. I. Guerrero-García, P. González-Mozuelos and M. O. De La Cruz, *J. Chem. Phys.*, 2011, **135**, 164705.
- 67 J. Wu, D. Bratko, H. Blanch and J. Prausnitz, *J. Chem. Phys.*, 1999, **111**, 7084–7094.
- 68 R. C. Van Lehn and A. Alexander-Katz, *J. Phys. Chem. A*, 2014, **118**, 5848–5856.
- 69 Y. Tu, M. Lv, P. Xiu, T. Huynh, M. Zhang, M. Castelli, Z. Liu, Q. Huang, C. Fan, H. Fang *et al.*, *Nat. Nanotechnol.*, 2013, **8**, 594.
- 70 R. C. Van Lehn and A. Alexander-Katz, *J. Phys. Chem. B*, 2014, **118**, 12586–12598.
- 71 X. Chen, D. P. Tieleman and Q. Liang, *Nanoscale*, 2018, **10**, 2481–2491.

We systematically study the aggregation of pH-responsive AuNPs and their interactions with model lipid bilayers by using the Martini coarse-grained molecular dynamics simulations.

